ISSN 0965-545X, Polymer Science, Series A, 2019, Vol. 61, No. 6, pp. 906–912. © Pleiades Publishing, Ltd., 2019.

COMPOSITES

The Influence of Soft-Epitaxial Crystallization on Polyamide 66/Carbon Nanotubes Composite Injection Bar

Enyi Chi[a], Minfang An[a], Guibin Yao[a], Yiguo Li[a], and Zongbao Wang[a,*]

[a] *Ningbo Key Laboratory of Specialty Polymers, Faculty of Materials Science and Chemical Engineering, Ningbo University, Ningbo, 315211 China*

**e-mail: wangzongbao@nbu.edu.cn*

Received June 25, 2019; revised July 15, 2019; accepted August 27, 2019

Abstract—The hydrogen–bonding-rich semi-crystalline polyamide 66 (PA66) was chosen to investigate the influence of soft-epitaxial effect on polymer/carbon nanotube (CNT) nanocomposite injection-molding bars, and the crystallization behavior was explored by differential scanning calorimeter (DSC), scanning electron microscope (SEM), two-dimensional wide angle X-ray diffraction (2D-WAXD) and two-dimensional small angle X-ray scattering (2D-SAXS). The results indicated that CNT is an effective nucleation agent for PA66 crystallization and the coupling of the flow and CNT can induce the soft-epitaxial crystallization of PA66 upon CNT surface, resulting in the coexistence of soft-epitaxial nanohybrid shish-kebab crystalline structure and conventional non-epitaxial crystals in PA66/CNT nanocomposites. Although the presence of CNT did not change the crystal structure of PA66, the generation and presence of soft-epitaxial crystals could feebly enhance the orientation degree of PA66 crystals and slightly improve the mechanical properties of PA66/CNT nanocomposites.

DOI: 10.1134/S0965545X20010022

INTRODUCTION

Polymer/inorganic nanocomposites possess new mechanical properties and novel functions relative to polymer matrix [1–7]. The interfacial interaction between inorganic nanofiller and polymer is the most important factor for polymer/inorganic nanocomposites [5, 8–10]. Four strategies, surface modification of the nanofiller [11–14], modification of the polymer [15], preparing polymer composites via in-situ polymerization method [16–18] and adding compatibilizer [19, 20] can improve the interfacial interaction between inorganic nanofiller and polymer. Thereto, the physical method can not only effectively enhance interfacial interaction but also avoid the destruction of the structure and properties of inorganic nanofiller. It has been proved that interfacial crystallization can effectively enhance interfacial interaction [21]. The soft-epitaxial crystallization, the same as the epitaxial crystallization, is a kind of interfacial crystallization. That the disregistry between the polymer crystal and the 2D epitaxial base is less than 15% is necessary during the epitaxial crystallization process [3, 6, 7]. During soft-epitaxial crystallization process, the polymer chains prefer to align along the tube axis regardless of the disregistry [2, 4, 13]. For example, 1D-carbon nanotubes (CNT) could induce the soft-epitaxial crystallization of semi-crystalline polymer on the surface of CNT. The strict lattice matching is not necessary while a cooperative orientation of the polymer chains and the CNT axes is needed.

In 1976, CNT were first observed [22]. CNT possess excellent mechanical and thermal properties, low mass density, large aspect ratio and the topological defects which exist in the surface of CNT for forming half dome [23]. A great number of researches have indicated that the crystallization of semi-crystalline polymer could soft-epitaxially grow on surface of CNT when the chains of semi-crystalline polymer were parallel to the surface of CNT. Meanwhile, nanohybrid shish-kebab structure was also observed using scanning electron microscope and transmission electron microscopy [24–27]. In nanohybrid shish-kebab structure, CNT replace the central fibril core of classic shish-kebab and is wrapped by disc-shaped polymer lamellar crystals. The nanohybrid shish-kebab structure of semi-crystalline polymer and CNT were studied by the controlled polymer solution crystallization method or physical vapor deposition technique. It has been reported that polyethylene, polyamide 66 (PA66), polyamide 6, poly(L-lysine) and polyvinylidene etc. could periodically form kebab crystals along the CNT axis [24, 25, 28, 29].

PA66 is widely used in engineering plastics because of its high thermal, mechanical properties, toughness and processability [30–32]. PA66 is typical hydrogen bonding rich semi-crystalline polymer. The crystal structure of PA66 is triclinic (α form), and the chain

adopts a planar zigzag conformation, and the lattice parameters of PA66 α-form crystal are $a = 0.49$ nm, $b = 0.54$ nm, $c = 1.72$ nm, $\alpha = 48.5°$, $\beta = 77°$, $\gamma = 63.5°$ [33]. Because the disregistry between the c-axis of PA66 crystal and the crystallographic parameter of ⟨2100⟩ RGO spacing is 0.1%, PA66 can epitaxial grow on the surface of RGO [34, 35]. Therefore, PA66 was chosen as the representative of hydrogen–bonding-rich semi-crystalline polymer to investigate the effect of soft-epitaxial crystallization in polymer/CNT nanocomposites.

Herein, we employed the injection molding to prepare test specimens in order to study the influence of CNT on the soft-epitaxial crystallization in PA66/CNT nanocomposites bar. We obtained pure PA66 (PA66) and 0.1 wt % CNT (PA66/CNT0.1), 0.5 wt % CNT (PA66/CNT0.5) and 1.0 wt % CNT (PA66/CNT1.0) nanocomposites by injection molding. We studied the structure of PA66/RGO nanocomposites by wide angle X-ray diffraction (WAXD), small angle X-ray scattering (SAXS), scanning electron microscope (SEM) and differential scanning calorimetry (DSC) measurements and compared their mechanical properties. The influence of soft-epitaxial crystallization on the crystal structure and the orientation, and the relationship between the soft-epitaxial crystallization and the mechanical property of PA66/CNT nanocomposites were discussed.

EXPERIMENTAL

Materials

PA66 (101L NC010) ($\rho = 1.14$ g/cm^3) (MFI: 2.0 (230°C/3.8 kg)) used in this work was purchased from DuPont Ltd. (USA). Multi-wall carbon nanotubes (CNT) with the length range of 5~20 μm were supplied by Alfa Aesar.

Analytical Methods

Differential scanning calorimetry (DSC) measurements were performed with Thermal Analyst Q1000 DSC under nitrogen atmosphere. All samples were heated to 280°C at a heating rate of 10 deg/min and equilibrated at 280°C for 3 min. Subsequently, the samples were cooled to 25°C at a cooling rate of 10 deg/min.

Two-dimensional wide angle X-ray diffraction (2D-WAXD) and two-dimensional small angle X-ray scattering (2D-SAXS) experiments were carried out on the BL16B1 beam-line in the Shanghai Synchrotron Radiation Facility (SSRF). The monochromatic X-ray wavelength was 1.239 Å, and the 2D patterns were recorded in transmission mode at room temperature. The sample-to-detector of 2D-WAXD experiment was 172.4 mm, and two different sample-to-detector distances of 5210 and 2320 mm were employed for 2D-SAXS experiments. The data of the WAXD and SAXS experiments were analyzed by the program FIT2D. By the program Xpolar developed by Stony Brook University, the crystallinity was acquired from 2D-WAXD.

For scanning electron microscope (SEM) observations, the PA66/CNT1.0 nanocomposites test specimen was first etched with 15% trichloroacetic acid then rinsed with ethyl alcohol. SEM experiment was carried out by using a Hitachi S-4800 field emission SEM operating at 10 kV.

Tensile test was performed on Instron 5567 at a tensile rate of 10 mm/min. Five standard bars for each sample were measured and the average values were calculated.

RESULTS AND DISCUSSION

DSC curves of pure PA66 and PA66/CNT nanocomposites are shown in Fig. 1. In all test specimens, the melting temperature T_m (Fig. 1) is fixed at about 263.5°C, while the crystallization temperatures T_c of pure PA66, PA66/CNT0.1, PA66/CNT0.5 and PA66/CNT1.0 are 232.8, 242.1, 244.1 and 244.2°C, respectively. The results suggest that CNT can provide heterogeneous nucleation sites for PA66 in the nanocomposites, but the T_m of pure PA66 and PA66/CNT nanocomposites is not increased. Based on the measured heat of fusion of pure PA66 (36.2 J/g), PA66/CNT0.1 (33.7 J/g), PA66/CNT0.5 (33.1 J/g) and PA66/CNT1.0 (39.7 J/g) from Fig. 1a, and according to the heat of fusion of 100% crystalline PA66 (188.4 J/g), [36, 37] the crystallinity of test samples are calculated to be 19.2, 17.8, 17.5, and 21.1%, respectively. The results show that the crystallinity of test specimens is not enhanced with the addition of CNT.

Figure 2 shows 2D-WAXD patterns obtained at the intermediate zones of all test specimens. The diffraction circles of the inner and the outward are designated to the (100) and (010) + (110) crystal planes of PA66 triclinic crystals, respectively [33]. Figure 3 shows 1D-WAXD curves of all test specimens collected from 2D-WAXD patterns (Fig. 2). The 2θ corresponding to (100) and (010) + (110) crystal planes are 16.3° and 19.0° in WAXD curves. Obviously, the crystal form of PA66/CNT nanocomposites is not affected with the addition of CNT. As shown in Fig. 4, the crystallinity of pure PA66, PA66/CNT0.1, PA66/CNT0.5 and PA66/CNT1.0 are 17.6, 17.1, 17.1, and 17.9%, respectively. The result of the crystalline degree calculated from WAXD results is consistent with that from DSC result. Therefore, we can conclude that the crystal structure of PA66 remains unchanged despite the presence of CNT in the PA66/CNT nanocomposites and the crystalline degree of all test specimens is not increased.

To further study the effect of CNT nanofiller on the crystal orientation, 3D-WAXD patterns were

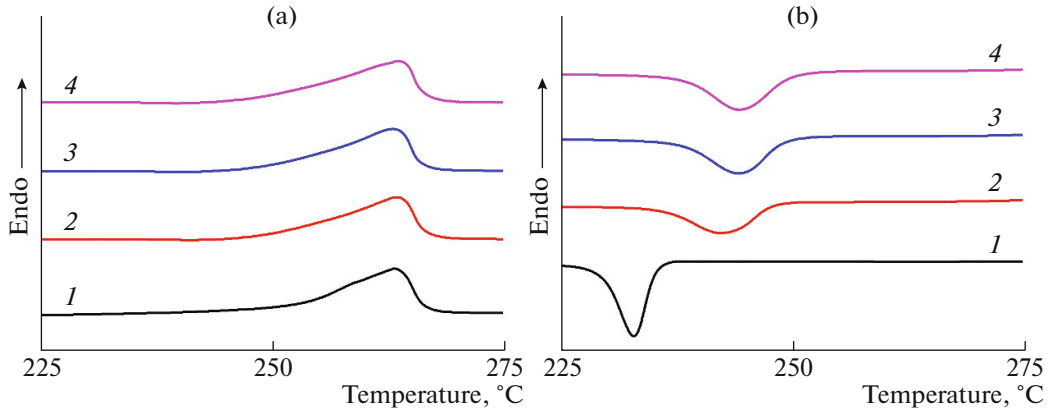

Fig. 1. (Color online) (a) The heating and (b) cooling curves of (*1*) pure PA66 and (*2*) PA66/CNT0.1, (*3*) PA66/CNT0.5, and (*4*) PA66/CNT1.0 nanocomposites.

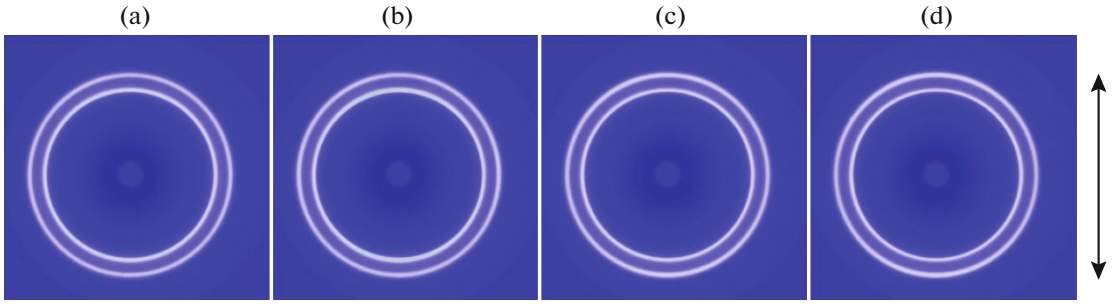

Fig. 2. (Color online) The 2D-WAXD parents of (a) pure PA66, (b) PA66/CNT0.1, (c) PA66/CNT0.5, and (d) PA66/CNT1.0. The direction of double-arrow was parallel to the flow direction.

obtained from Fig. 2. As can be seen from Fig. 5, with the increase of CNT contents, the intensity and orientation of the two crystal diffraction rings changed in 3D-WAXD patterns, although the two diffraction rings have no obvious change in 2D-WAXD patterns (Fig. 2). In 3D-WAXD pattern, the orientation of (010) crystal plane are feebly enhanced along the flow direction, when CNT are added into the matrix.

SAXS was also used to investigate the structure of PA66/CNT nanocomposites. Figure 6 shows 2D-SAXS patterns of the test specimens. Because the crystallinity of the test specimens is low, the scattered signal is weak. In 2D-SAXS patterns, the scattered signals can be divided into the center signal which is collected near the beam stop and the outer signal which is collected near the edge of the detector. The Lorenz-corrected SAXS curves were collected from 2D-SAXS patterns, as shown in Fig. 7a. The Lorenz-corrected curves of the test specimens have multiple scattering peaks with exception of pure PA66. In the Lorenz-corrected curves, q_1 and q_2 respectively represent the first and second scattering peak positions. The q_1 peak does not appear in the Lorenz-corrected curves of pure PA66, but the intension of q_1 peak of PA66/CNT nanocomposites increases with the addition of CNT. The addition of CNT brings PA66 nanocomposites to form the new period structure. The value of q_2 was collected from the SAXS curves of sample-to-detector distance of 2320 mm (Fig. 7b). The intension of q_2

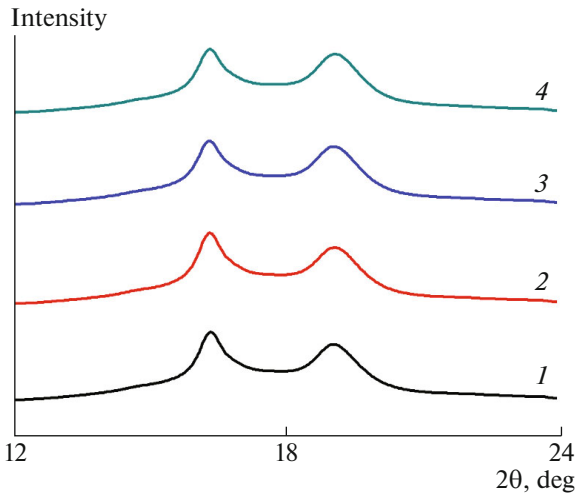

Fig. 3. (Color online) The 1D-WAXD curves of (*1*) pure PA66 and (*2*) PA66/CNT0.1, (*3*) PA66/CNT0.5, and (*4*) PA66/CNT1.0 nanocomposites.

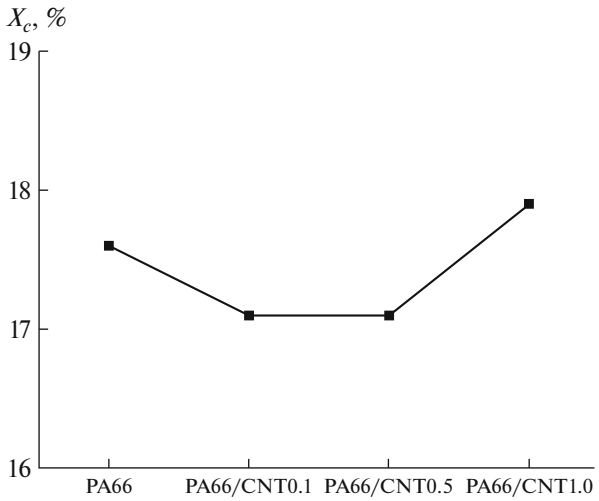

Fig. 4. The crystallinity of pure PA66 and PA66/CNT0.1, PA66/CNT0.5, and PA66/CNT1.0 nanocomposites.

peak declines gradually with increase of CNT. The long period of the test specimens was calculated using the Bragg equation, $L = 2\pi/q$, where L is the long period, and q represents the peak position in the scattering curves. L_1 and L_2 are calculated to be 62.83 and 7.85 nm, respectively. It has been reported that PA66 can periodically form kebab crystals along the CNT axes because of soft-epitaxial crystallization, [24, 25, 28, 29] namely form nanohybrid shish-kebab structure. The long period of soft-epitaxial crystal is not dependent on the thickness of lamellae and amorphous layer as usual non-epitaxial lamellar crystals, but on the distance between the kebab crystals on CNT. Therefore, the long period of soft-epitaxial crystal is generally much larger than the usual non-epitaxial crystals. In the chosen samples, there is not other source of long period except for the PA66 crystals. Therefore, L_1 and L_2 are connected with the period structures of soft-epitaxial crystal and non-epitaxial crystal, respectively. Further, the results were analyzed using Electron density correlation function. The crystal thickness (*dc*) of soft-epitaxial crystal is calculated to be 20.47 nm. It matches with the results of the controlled polymer solution crystallization method or physical vapor deposition technique [24, 29]. Therefore, the addition of CNT can bring PA66/CNT nanocomposites to generate the new period structure originating from the existence of soft-epitaxial crystallization.

The 2D-SAXS was used to study the orientation of the test specimens. The azimuthally integrated profile of Fig. 8 was collected from the outer and center signals of 2D-SAXS patterns, respectively. As can be seen in Fig. 8a, the signal intensity of outer signal weakens with the increase of CNT content. As shown in Fig. 8b, the center signal intensity of 2D-SAXS enhances with the increase of CNT content. And the signal distributions of PA66/CNT0.5 and PA66/CNT1.0 composites have two weak peaks at 90° and 180°, the same as the signal distributions of Fig. 8b. Therefore, the addition of CNT can induce the slight orientation of PA66/CNT nanocomposites. It is consistent with the results of WAXD.

In high-crystalline poly(vinyl alcohol)/CNT and polyethylene/CNT nanocomposites, the coexistence of numerous soft-epitaxial crystals and non-epitaxial crystals can improve the mechanical properties [38, 39]. In Fig. 9, the tensile strength of pure PA66, PA66/CNT0.1, PA66/CNT0.5 and PA66/CNT1.0 nanocomposites are 74.3 ± 2.8, 74.6 ± 2.2, 75.2 ± 2.2, and 76.7 ± 2.4 MPa, respectively. It indicates that the soft-epitaxial crystals can lightly influence the mechanical properties of nanocomposites. It is known that a lot of hydrogen bonds exist in the crystalline and amorphous region of PA66. In stretching process, the crystals and the hydrogen bonding amorphous phase together resist the strain. The existence of CNT destroys the consecutiveness of hydrogen bonds in the amorphous phase of PA66 matrix. Giti Pishehvarz et al. obtained similar conclusion by molecular dynamics simulation [40]. However, the amount of CNT, soft-epitaxial crystals and non-epitaxial crystals are fewer comparing to hydrogen bonding in PA66 matrix, therefore the tensile strength of PA66/CNT nanocomposites are weakly enhanced.

As the test specimens in our study are injection-molding samples, the crystallization process of specimens is non-isothermal crystallization with the influence of intensive flow field. It is well known that shish-

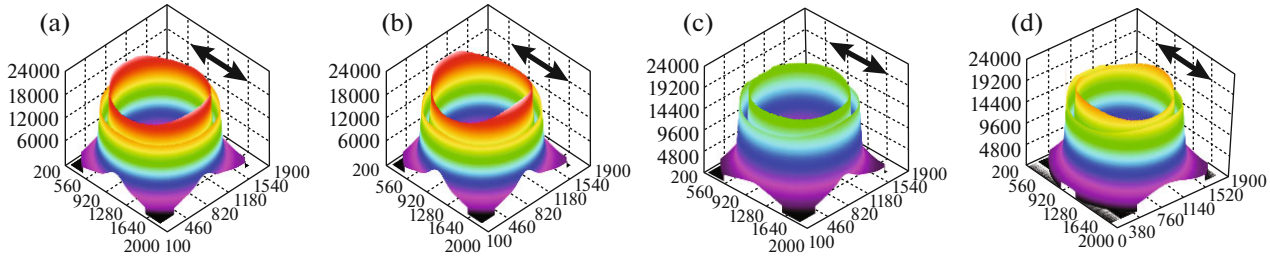

Fig. 5. (Color online) The 3D-WAXD parents of (a) pure PA66, (b) PA66/CNT0.1, (c) PA66/CNT0.5, and (d) PA66/CNT1.0. The direction of double-arrow was parallel to the flow direction.

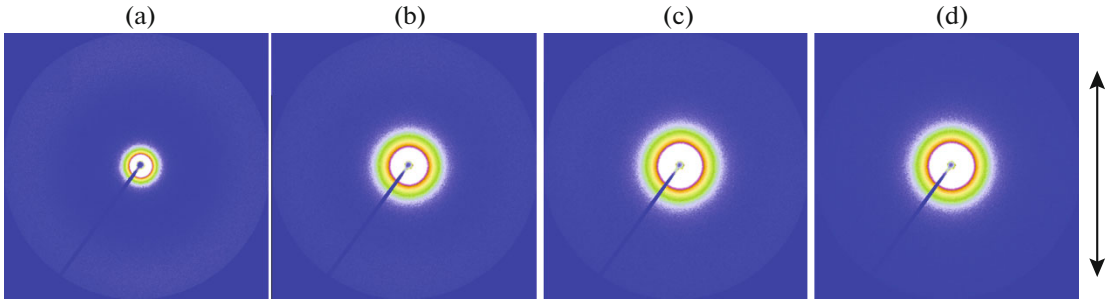

Fig. 6. (Color online) The 2D-SAXS patterns of (a) pure PA66, (b) PA66/CNT0.1, (c) PA66/CNT0.5, and (d) PA66/CNT1.0. The sample-to-detector distance was 5210 mm. The direction of double-arrow was parallel to the flow direction.

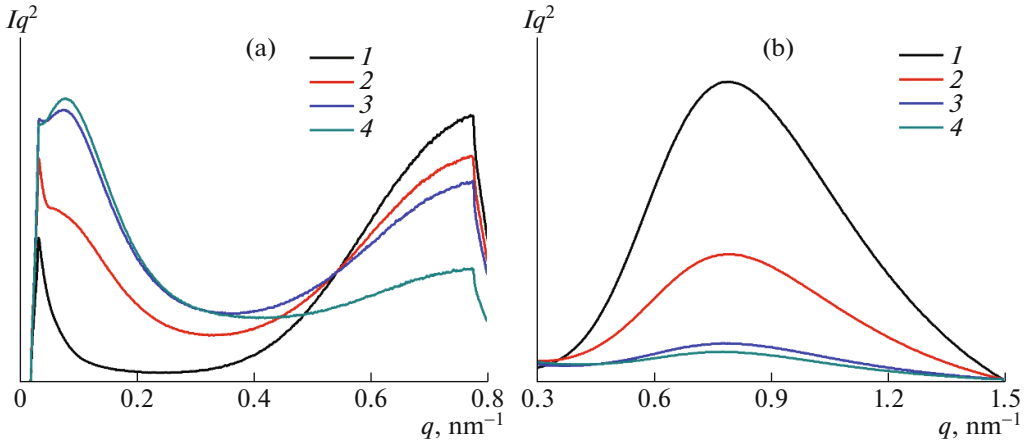

Fig. 7. (Color online) The Lorentz-corrected SAXS curves of (*1*) pure PA66 and (*2*) PA66/CNT0.1, (*3*) PA66/CNT0.5, and (*4*) PA66/CNT1.0 nanocomposites. (a) The sample-to-detector distance was 5210 mm. (b) The sample-to-detector distance was 2320 mm.

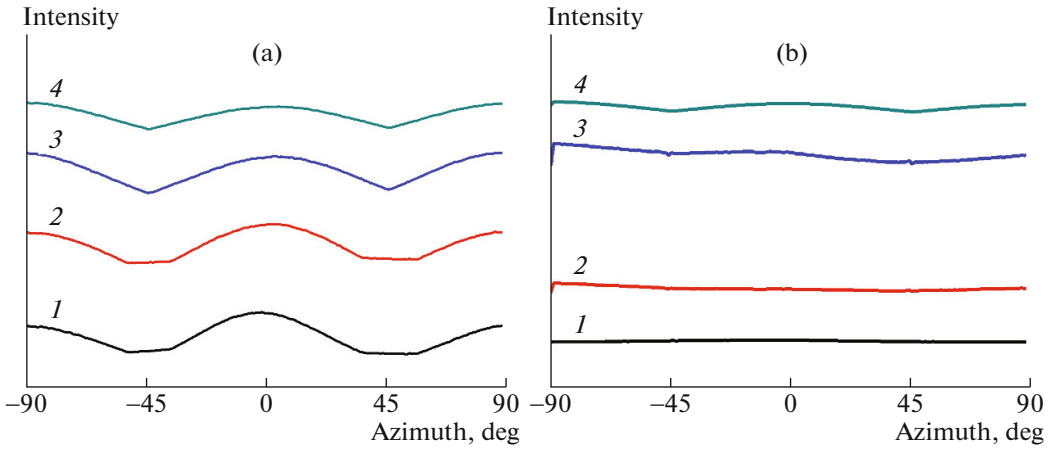

Fig. 8. (Color online) The origin (angle = 0) of the azimuthal angle is the positive direction of equator line in 2D SAXS pattern. Respectively, the q range of integration of outer scattering signal and center scattering signal is 0.4–1.5 and 0–0.3 nm^{-1}. Azimuthally integrated profiles of (a) outer scattering signal and (b) center scattering signal of (*1*) pure PA66 and (*2*) PA66/CNT0.1, (*3*) PA66/CNT0.5, and (*4*) PA66/CNT1.0 nanocomposites.

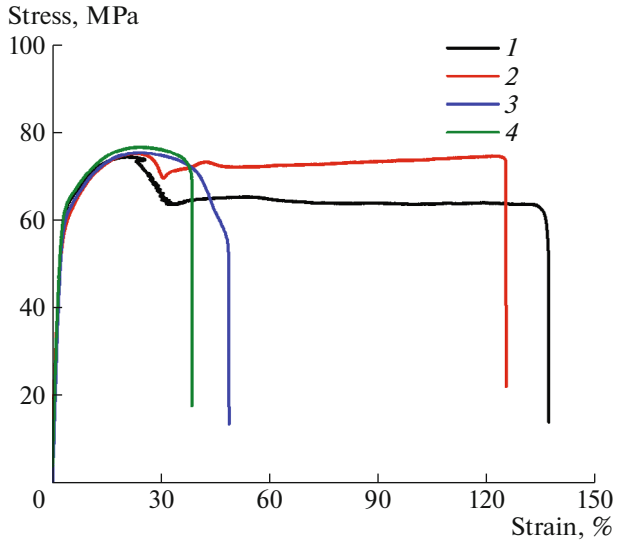

Fig. 9. (Color online) Stress-strain curves of (*1*) pure PA66 and (*2*) PA66/CNT0, (*3*) PA66/CNT0.5, and (*4*) PA66/CNT1.0 nanocomposites.

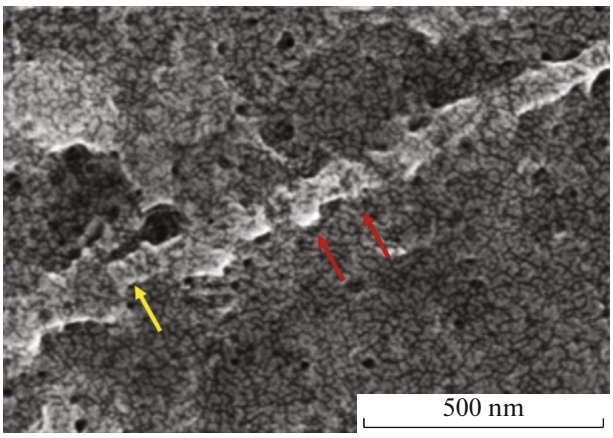

Fig. 10. (Color online) SEM images of etched PA66/CNT1.0 nanocomposites. The kebab crystals of PA66 were pointed out by red arrow. The CNT were pointed out by yellow arrow.

kebab structure can form in certain polymer melt under strong shear or stretch field. In the preparation of PA66/CNT nanocomposites, CNT provide a 1D nucleation structure and the oriented nanohybrid shish-kebab structure can form [41]. Because of the existence of intensive flow field in the injection molding process, PA66 chains and CNT are apt to parallel to the flow direction, and CNT can adsorb PA66 chains. In non-isothermal crystallization process, PA66 chains periodically form kebab crystals along the CNT axes. In the process, CNT are a substitute for the stretched chains in classic polymer shish-kebab crystals and provide the base for the soft-epitaxial crystal of PA66 matrix. The formation of shish-kebab structure with soft-epitaxial growth in other semi-crystalline polymer on the surface of CNT has been observed by the controlled polymer solution crystallization method or physical vapor deposition technique [24, 26, 27, 29, 41, 42]. Therefore, the degree of orientation of PA66/CNT nanocomposites is enhanced along the flow direction with the increase of the amount of CNT, as shown in Fig. 5. As the amount of CNT is increased, the soft-epitaxial crystals gradually become the main portion of PA66 crystal for the crystallinity of whole PA66 sample is low. It is easily understood that CNT nanofiller, according to the WAXD results, does not enhance the crystalline degree of PA66 matrix and does not change the crystal structure since even RGO with strict epitaxial crystallization with PA66 has not achieve [34]. It is concluded that the nanohybrid shish-kebab crystalline structure exists in test specimens and the soft-epitaxial crystals are much greater than the non-epitaxial crystals because CNT and intensive flow field exist in PA66/CNT nanocomposites preparation process. The SAXS results are also consistent with the conclusion above. q_1 and q_2 in Fig. 7a respectively represent the different period structure in pure PA66 and its nanocomposites. Because the SAXS curve of pure PA66 has only one peak and L_2 is about 7.85 nm, L_2 should represent the period structure of the non-epitaxial crystal. As CNT are added, the other long period (L_1 = 62.83 nm) arises. To further confirm the existence of shish-kebab structure in PA66/CNT nanocomposites, the PA66/CNT1.0 composite injection bar was etched by trichloroacetic acid. In Fig. 10, the lamellae of PA66 matrix are observed on the surface of CNT. Apparently, L_1 is the period structure of adjacent soft-epitaxial crystals and the crystal size of soft-epitaxial crystal is measured to be about 20 nm. Recollected the SAXS result that the *dc* is 20.47 nm in PA66/CNT nanocomposites, which indicates that soft-epitaxial effect can enhance the crystal thickness of PA66 matrix. Therefore, the crystals of PA66/CNT nanocomposites include the soft-epitaxial and non-epitaxial crystals and the amount of soft-epitaxial crystals is greater than that of non-epitaxial crystals. These results indicate that the crystal structure and the crystallinity of PA66 matrix are unchanged but the kebab lamellae replace a part of the non-epitaxial crystals under the influence of soft-epitaxial effect with the addition of CNT.

CONCLUSIONS

The preparation process of test specimens is the injection molding in the study. In non-isothermal crystallization process, the nanohybrid shish-kebab structure is observed under the influence of the soft-epitaxial crystallization. The soft-epitaxial crystals and the non-epitaxial crystals coexist in the PA66/CNT nanocomposites. 1D CNT nanofiller does not influence the crystal structure of PA66

matrix. CNT are a nucleation agents to assist the crystallization of PA66 resulting in generation of soft-epitaxial crystals and can enhance the orientation degree of PA66 chains in PA66/CNT nanocomposites. The size of soft-epitaxial crystals is greater than that of non-epitaxial crystals. The soft-epitaxial crystals can slightly influence the mechanical properties of nanocomposites.

ACKNOWLEDGMENTS

This work was supported by the National Natural Science Foundation of China (U1532114, 51773101), and K. C. Wong Magna Fund in Ningbo University. We thank Shanghai Synchrotron Radiation Facility (SSRF) for supporting the SAXS and WAXD test.

REFERENCES

1. D. H. Gray, S. L. Hu, E. Juang, and D. L. Gin, Adv. Mater. **9**(9), 731 (1997).
2. M. Rahmat and P. Hubert, Compos. Sci. Technol. **72**(1), 72 (2011).
3. Y. Takenaka, H. Miyaji, A. Hoshino, A. Tracz, J. K. Jeszka, and I. Kucinska, Macromolecules **37**(26), 9667 (2004).
4. C. Y. Li, L. Li, W. Cai, S. L. Kodjie, and K. K. Tenneti, Adv. Mater. **17**(9), 1198 (2010).
5. J. Petermann, G. Broza, U. Rieck, and A. Kawaguchi, J. Mater. Sci. **22**(4), 1477 (1987).
6. B. Wang, Y. Zhang, J. Zhang, H. Li, P. Chen, Z. Wang, and Q. Gu, Ind. Eng. Chem. Res. **52**(45), 15824 (2013).
7. B. J. Wang, Y. G. Li, G. S. Weng, Z. Q. Jiang, P. Chen, Z. B. Wang, and Q. Gu, Compos. Sci. Technol. **96**, 63 (2014).
8. J. Petermann and Y. Xu, Colloid Polym. Sci. **269**(5), 455 (1991).
9. B. Gross and J. Peterman, J. Mater. Sci. **19**(1), 105 (1984).
10. N. Ning, S. Fu, W. Zhang, F. Chen, K. Wang, H. Deng, Q. Zhang, and Q. Fu, Prog. Polym. Sci. **37**(10), 1425 (2012).
11. T. Ramanathan, A. A. Abdala, S. Stankovich, D. A. Dikin, M. Herrera-Alonso, R. D. Piner, D. H. Adamson, H. C. Schniepp, X. Chen, R. S. Ruoff, S. T. Nguyen, I. A. Aksay, R. K. Prud'homme, and L. C. Brinson, Nature Nanotechnol. **3**(6), 327 (2008).
12. Y. Deng, Y. J. Li, J. Dai, M. D. Lang, and X. Y. Huang, J. Polym. Sci. Part A: Polym. Chem. **49**(7), 1582 (2011).
13. B.-X. Yang, K. P. Pramoda, G. Q. Xu, and S. H. Goh, Adv. Funct. Mater. **17**(13), 2062 (2007).
14. Y. W. Cao, Z. L. Lai, J. C. Feng, and P. Y. Wu, J. Mater. Chem. **21**(25), 9271 (2011).
15. H. J. Salavagione and G. Martinez, Macromolecules **44**(8), 2685 (2011).
16. L. Feng, Z. Zhou, A. Dufresne, J. Huang, M. Wei, and L. An, J. Appl. Polym. Sci. **112**(5), 2830 (2009).
17. H. Hu, X. Wang, J. Wang, L. Wan, F. Liu, H. Zheng, R. Chen, and C. Xu, Chem. Phys. Lett. **484**(4–6), 247 (2010).
18. T. Sun and J. M. Garces, Adv. Mater. **14**(2), 128 (2002).
19. H.-S. Kim, B.-H. Lee, S.-W. Choi, S. Kim, and H.-J. Kim, Compos. Part A: Appl. Sci. Manufact. **38**(6), 1473 (2007).
20. H. Li and S. Yan, Macromolecules **44**(3), 417 (2011).
21. N. Y. Ning, S. R. Fu, W. Zhang, F. Chen, K. Wang, H. Deng, Q. Zhang, and Q. Fu, Prog. Polym. Sci. **37**(10), 1425 (2012).
22. S. Iijima, Nature **354**, 56 (1991).
23. P. J. F. Harris, A. E. Hern, and N. I. Yakobson, Am. J. Phys. **72**(3), 787 (2001).
24. L. Li and C. Li, J. Am. Chem. Soc. **128**(5), 1692 (2006).
25. S. Kodjie, L. Li; B. Li, W. Cai, C. Li, and K. Mimi, J. Macromol. Sci. Part B **45**(2), 231 (2006).
26. L. Wang, X. Dong, M. Huang, and D. Wang, Polymer **97**, 217 (2016).
27. T. Kamal, S. Y. Park, M. C. Choi, Y. W. Chang, W. T. Chuang, and U. S. Jeng, Polymer **53**(15), 3360 (2012).
28. C. Y. Li, L. Y. Li, W. W. Cai, S. L. Kodjie, and K. K. Tenneti, Adv. Mater. **17**(9), 1198 (2005).
29. L. Li, Y. Yang, G. Yang, X. Chen, B. S. Hsiao, B. Chu, J. E. Spanier, and C. Y. Li, Nano Lett. **6**(5), 1007 (2006).
30. H. L. Qin, Q. S. Su, S. M. Zhang, B. Zhao, and M. S. Yang, Polymer **44**(24), 7533 (2003).
31. L. Song, Y. Hu, Q. He, and F. You, J. Fire Sci. **26**(6), 475 (2008).
32. E. M. Araujo, K. D. Araujo, R. A. Paz, T. R. Gouveia, R. Barbosa, and E. N. Ito, Journal of Nanomaterials 2009, 136856 (2009).
33. C. W. Bunn and E. V. Garner, Proceedings of the Royal Society A **189**(1016), 39 (1947).
34. E. Chi, M. An, G. Yao, F. Tian, and Z. Wang, Crystals **7**(12), 384 (2017).
35. J. C. Meyer, A. K. Geim, M. I. Katsnelson, K. S. Novoselov, T. J. Booth, and S. T. Roth, Nature **446**(7131), 60 (2007).
36. D. Garcia and H. W. Starkweather Jr., J. Polym. Sci. Part B: Polym. Phys. **23**(3), 537 (1985).
37. L. T. Lim, I. J. Britt, and M. A. Tung, J. Appl. Polym. Sci. **71**(2), 197 (1999).
38. B. Vigolo, A. Pénicaud, C. Coulon, C. Sauder, R. Pailler, C. Journet, P. Bernier, and P. Poulin, Science **290**(5495), 1331 (2000).
39. R. Haggenmuller, W. Zhou, J. E. Fischer, and K. I. Winey, J. Nanosci. Nanotechnol. **3**(1–2), 105 (2003).
40. G. Pishehvarz, H. Erfan-Niya, and E. Zaminpayma, Comput. Mater. Sci. **155**, 499 (2018).
41. H. Koerner, J. J. Kelley, and R. A. Vaia, Macromolecules **41**(13), 4709 (2008).
42. M. Moniruzzaman, A. Sahin, and K. I. Winey, Carbon **47**(3), 645 (2009).